Metadata of the chapter that will be visualized in SpringerLink

Book Title	A Systems Theoretic Approach to Systems and Synthetic Biology II: Analysis and Design of Cellular Systems	
Series Title		
Chapter Title	Modelling and Analysis of Feedback Control Mechanisms Underlying Osmoregulation in Yeast	
Copyright Year	2014	
Copyright HolderName	Springer Science+Business Media Dordrecht	
Corresponding Author	Family Name	**Montefusco**
	Particle	
	Given Name	**Francesco**
	Prefix	
	Suffix	
	Division	Centre for Systems, Dynamics and Control, College of Engineering, Mathematics and Physical Sciences
	Organization	University of Exeter
	Address	Exeter, UK
	Email	f.montefusco@exeter.ac.uk
Author	Family Name	**Akman**
	Particle	
	Given Name	**Ozgur E.**
	Prefix	
	Suffix	
	Division	Centre for Systems, Dynamics and Control, College of Engineering, Mathematics and Physical Sciences
	Organization	University of Exeter
	Address	Exeter, UK
	Email	o.e.akman@exeter.ac.uk
Author	Family Name	**Soyer**
	Particle	
	Given Name	**Orkun S.**
	Prefix	
	Suffix	
	Division	Centre for Systems, Dynamics and Control, College of Engineering, Mathematics and Physical Sciences
	Organization	University of Exeter
	Address	Exeter, UK
	Email	o.s.soyer@exeter.ac.uk
Author	Family Name	**Bates**
	Particle	
	Given Name	**Declan G.**
	Prefix	
	Suffix	

Division	Centre for Systems, Dynamics and Control, College of Engineering, Mathematics and Physical Sciences
Organization	University of Exeter
Address	Exeter, UK
Email	d.g.bates@exeter.ac.uk

Abstract	Biological systems display complex dynamics emerging from intricate networks of interacting molecular components: cells use signalling pathways and regulatory control mechanisms to coordinate multiple processes, allowing them to respond and adapt to an ever-changing environment. Many structural and dynamical features of biological control systems can also be found in engineered control systems and, hence, feedback control theory can provide a useful approach for the analysis and design of complex biological systems. In this chapter we provide a control theoretic analysis of the osmoregulation system in *Saccharomyces cerevisiae* (see [8, 24, 26, 40]), where a complex biochemical signalling and regulatory network allows cells to maintain homeostasis in the face of osmotic shock.

Keywords (separated by '-')	Osmoregulation - Signalling pathway - Signaling pathway - Homeostasis - Osmosis - Osmoadaptation - Eukaryotic - Yeast - High osmolarity glycerol (HOG) - Integral feedback

Chapter 4
Modelling and Analysis of Feedback Control Mechanisms Underlying Osmoregulation in Yeast

Francesco Montefusco, Ozgur E. Akman, Orkun S. Soyer and Declan G. Bates

Abstract Biological systems display complex dynamics emerging from intricate networks of interacting molecular components: cells use signalling pathways and regulatory control mechanisms to coordinate multiple processes, allowing them to respond and adapt to an ever-changing environment. Many structural and dynamical features of biological control systems can also be found in engineered control systems and, hence, feedback control theory can provide a useful approach for the analysis and design of complex biological systems. In this chapter we provide a control theoretic analysis of the osmoregulation system in *Saccharomyces cerevisiae* (see [8, 24, 26, 40]), where a complex biochemical signalling and regulatory network allows cells to maintain homeostasis in the face of osmotic shock.

Keywords Osmoregulation · Signalling pathway · Signaling pathway · Homeostasis · Osmosis · Osmoadaptation · Eukaryotic · Yeast · High osmolarity glycerol (HOG) · Integral feedback

F. Montefusco (✉) · O. E. Akman · O. S. Soyer · D. G. Bates
Centre for Systems, Dynamics and Control, College of Engineering, Mathematics and Physical Sciences, University of Exeter, Exeter, UK
e-mail: f.montefusco@exeter.ac.uk

O. E. Akman
e-mail: o.e.akman@exeter.ac.uk

O. S. Soyer
e-mail: o.s.soyer@exeter.ac.uk

D. G. Bates
e-mail: d.g.bates@exeter.ac.uk

V. V. Kulkarni et al. (eds.), *A Systems Theoretic Approach to Systems and Synthetic Biology II: Analysis and Design of Cellular Systems*, DOI: 10.1007/978-94-017-9047-5_4,

324129_1_En_4_Chapter ☑ TYPESET ☐ DISK ☐ LE ☑ CP Disp.:15/5/2014 Pages: 34 Layout: T1-Standard

4.1 Introduction

Osmosis is the diffusion of water through a semipermeable membrane (permeable to the solvent, but not the solute), from the compartment containing a low concentration (hypotonic) solution to the one at high concentration (hypertonic). The chemical potential of water is central in this process and can be considered as a measure of the effective water concentration in a given area. The water potential is influenced by two factors, [17]: the osmotic potential and the pressure potential. The first is approximately proportional to the concentration of dissolved molecules of solutes: when the concentration of solute molecules increases, the water potential decreases. The second takes into account the hydrostatic pressure, the pressure exerted by a fluid at equilibrium due to the force of gravity. For two regions of water with different potentials and separated from each other by a semipermeable membrane, there is a water flow to the region of lower potential by osmosis: the movement of the fluid from the hypotonic to the hypertonic solution, while decreasing the concentration difference, increases the pressure of the hypertonic solution with respect to the hypotonic, thus producing a force that counteracts the osmosis. When these two effects balance each other, the osmotic equilibrium is reached: there is no net movement of solvent and the pressure required to maintain an equilibrium is defined as the osmotic pressure.

Osmosis is particularly important for cells, since many biological membranes are permeable to small molecules like water, but impermeable to larger molecules and ions. Osmosis provides the primary means by which water is transported into and out of cells. Typically, a cell has a higher intra cellular osmotic pressure (P_i) than extra cellular osmotic pressure (P_e). The main reason for this difference is that highly charged macromolecules and metabolites attract many small inorganic ions to the cell interior (the Donnan effect, see [1]). Due to this difference, water will flow into the cell, leading to swelling and potentially to cell rupture. The yeast *Saccharomyces cerevisiae* prevents the fundamental problem of water inflow and cell swelling by its cell wall, which is less elastic than the plasma membrane. The cell wall resists the expansion of the cell and creates an inward pressure on the cell contents, Gervais and Beney [9]. This pressure is called the turgor pressure P_t, defined as the difference in the hydrostatic pressure between the inside and the outside of the cell. At equilibrium (equil.), the water potential is equal inside and outside of the cell and the turgor pressure balances the difference in osmotic pressures, as in [33],

$$P_i = P_e + P_t \qquad (equil.). \tag{4.1}$$

Osmotic shocks arise due to a sudden rise (for example the addition of salt to the cell medium) or fall in the concentration of a solute in the cell's environment, resulting in rapid movements of water through the cell's membrane. These movements can produce dramatic consequences for the cell, since loss of water inhibits the transport of substrates and cofactors into the cell, while the uptake of large quantities of water can lead to swelling, rupture of the cell membrane or apoptosis. Due to their more

direct contact with their environment, single-celled organisms are generally more vulnerable to osmotic shock. However, cells in large animals such as mammals also suffer similar stresses under certain conditions, Ho [12].

Osmoadaptation is the mechanism by which cells sense and respond to various changes in their environmental conditions to avoid the aforementioned dramatic consequences. Organisms have evolved a variety of mechanisms to respond to osmotic shock. Typically, cells recognise changes in the osmolarity of their surroundings by using surface sensors which generate signals by activating signal transduction networks. These pathway are found in all eukaryotic organisms and are important in coordinating the response from the cell membrane into the cell, Rep et al. [30]. Recent experimental research indicates that most eukaryotic cells use the mitogen activated protein (MAP) kinase pathways for this purpose, Kltz and Burg [16].

4.2 Osmoregulation Process in Yeast

In recent years, the osmoregulatory response in yeast has emerged as an important model system for studying adaptive, homeostatic responses to environmental disturbances (see [8, 15]). The underlying molecular control system is well characterized in *Saccharomyces cerevisiae* (see [26, 40]), where it comprises three separate mechanisms that act to adjust the glycerol production in order to keep the cell's turgor pressure and volume constant in the face of environmental changes: (1) the regulation of the membrane protein Fps1 determining the glycerol export rate; (2) the transcription of several genes, whose proteins are involved in glycerol production, by the activation of the high osmolarity glycerol (HOG) mitogen-activated protein kinase (MAPK) signaling pathway and (3) the HOG kinase dependent regulation of the glycerol via non-transcriptional mechanisms. Despite its biochemical complexity (see Fig. 4.1), the osmoregulation system in yeast can be naturally abstracted as a feedback control system comprised of distinct branches as described above. This approach was taken in recent studies, which aimed to use standard engineering control models to capture the experimentally observed responses of yeast to osmotic shock and to further predict its structural and dynamic features (see [8, 24, 26]). Gennemark et al. [8] combined proportional controllers to model the above-described biochemical branches. Mettetal et al. [24] developed a concise model by using linear systems theory, and then revised this model arguing for the necessity of at least one branch of the system to implement integral control to achieve the experimentally observed adaptive responses in the system, Muzzey et al. [26]. The role of integral feedback in perfectly adaptive systems is by now well-studied in the Systems Biology literature (see [26, 27]), and it is highly likely that the osmoregulation system in yeast does indeed include a biochemical implementation of integral feedback, as seen in other systems (see [6, 27, 39]). It is still unclear, however, exactly how biological control systems such as osmoregulation might have evolved to use integral feedback control, and whether other alternative mechanisms might produce similar (or better) performance properties.

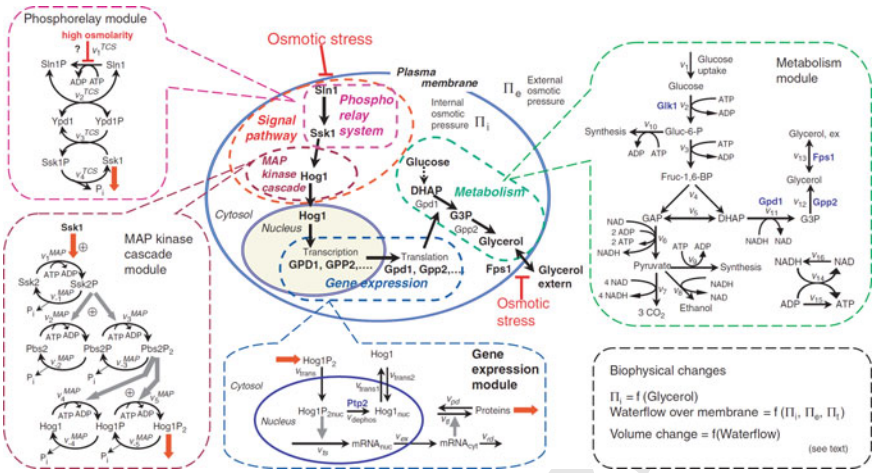

Fig. 4.1 Overview of the response of yeast to osmotic schlock, the figure has been taken from [15] and reproduced with permission of Nature Publishing Group

As a first step towards answering this question, we recently extended the proportional controller model devised in [8] with the implementation of an ultrasensitive controller, Montefusco et al. [25]. Ultrasensitivity describes a particular form of sensitivity in biological systems, where the system does not respond to incoming signals outside of a certain regime, but responds in a highly sensitive manner within this regime. Such an input-output relationship (i.e. ultrasensitivity) can be described by a specific nonlinear function, is shown to be a ubiquitous feature in several biological systems, and can be biochemically implemented through a variety of mechanisms such as phosphorylation cycles and cooperative binding (see [4, 11]). The MAPK systems, which are also found in osmoregulation, are theoretically shown to be capable of embedding ultrasensitivity (see [3, 13]), and bistability [21]. Starting from the proportional control model developed by [8], we explore the consequences of such potential ultrasensitivity and show that it significantly increases system performance in achieving homeostasis to osmotic perturbations.

In the following sections we present the model devised in [8], then we focus our attention on the results presented in [24, 26]. Finally, we provide an updated description of the recent results first presented in [25].

4.3 A Proportional Control Based Model of the Osmoregulation in Yeast

In this section we describe the model presented in [8], where the authors devised a simple ordinary differential equation (ODE) model of the adaptive response to an osmotic shock in *S. cerevisiae*. They abstracted several elements to yield a reduced

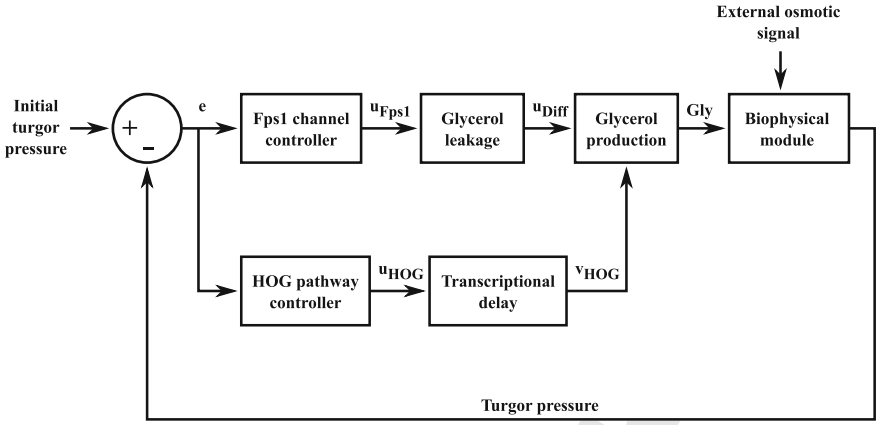

Fig. 4.2 Mathematical model of the osmoregulation process. This figure has been adapted from [8]

representation of the system, starting from the detailed model developed in [15] (see the diagram in Fig. 4.2). The model, in particular, consists of two main components. First, a biophysical model describing how the cell volume and the turgor pressure are affected by varying extra–cellular osmolarity. Second, the two parallel mechanisms for controlling the biophysical system in order to keep turgor pressure and volume constant: one by controlling the production of glycerol via the HOG pathway and the other by controlling the outflow of glycerol via the Fps1 channel. The complete model consists of 4 ODE's, 3 algebraic equations and 10 parameters, that have been estimated using experimental data on glycerol. The authors have validated the model by predicting the behaviour of modified strains and input functions.

4.3.1 The Mathematical Model

The mathematical model presented in [8] is described in the following paragraphs.

4.3.1.1 The Biophysical Module

The biophysical system is modelled by considering the dependencies between cell volume V, the turgor pressure P_t, the intra–cellular osmotic pressure P_i and the extra–cellular osmotic pressure P_e. At any given time t, $P_i(t)$, $P_e(t)$ and $P_t(t)$ are determining the flow of water across the cell membrane, which is proportional to $(P_i(t) - P_e(t) - P_t(t))$. Assuming that the cell volume is only affected by the inflow and outflow of water, then the change in volume can be expressed as

$$\frac{dV}{dt} = k_{p1}(P_i(t) - P_e(t) - P_t(t)), \tag{4.2}$$

with k_{p1} denoting a hydraulic water permeability constant. At equilibrium (equil.), i.e. constant volume and no net flow of water over the membrane, the Eq. (4.2) reduces to (4.1).

The only osmolyte considered explicitly in the model is glycerol (Gly) and, hence, ions and other small molecules, changing upon osmotic shock, Sunder et al. [35], are not considered. This assumption is motivated by experimental results from [29], where the authors found that glycerol counter-balances approximately 80 % of applied NaCl in *S. cerevisiae*. Therefore, the intra-cellular osmotic pressure, according to van't Hoff's law, is expressed as

$$P_i(t) = \frac{s + Gly(t)}{V(t) - V_b}, \tag{4.3}$$

with s being the concentration of the sum of osmolytes (assumed constant) other than glycerol present in the cell, and V_b being the non-osmotic volume of the cell, subsuming non-polar cellular components, such as membranes. According to Eq. (4.3), the intra–cellular osmotic pressure increases with the glycerol, which can be used to control the turgor pressure of the cell. The extra-cellular osmotic pressure is only modified by the input signal, for example applied salt stress, and is then independent of changes in other variables. The turgor pressure is linearly dependent on the volume according to [17], in the following manner:

$$P_t(t) = \varepsilon \left(\frac{V(t)}{V(0)} - 1 \right) + P_t(0), \tag{4.4}$$

where $V(0)$ is the initial volume, $P_t(0)$ is the initial turgor pressure, and ε is the volumetric elastic modulus. By expressing the volume at which $P_t = 0$ with the notation $V^{P_t=0}$, (4.4) can be rewritten as

$$P_t(t) = \begin{cases} P_t(0) \frac{V(t) - V^{P_t=0}}{V(0) - V^{P_t=0}}, & V(t) > V^{P_t=0} \\ 0, & \text{otherwise.} \end{cases}$$

4.3.1.2 The Controller Modules

There are two branches of control in the model: the first represents the closure of Fps1 glycerol transporter channels as a reaction to osmotic shock, and the second the activation of the HOG pathway, leading to glycerol production after a time delay. The input signal e arriving at the controllers is expressed as

$$e(t) = P_t(0) - P_t(t), \tag{4.5}$$

which is the difference in turgor pressure. The output of the Fps1 branch, which corresponds to the response of the transporter channels, is given by

$$u_{Fps1}(t) = \begin{cases} k_{p2}\frac{P_t(0)-e(t)}{P_t(0)}, & e(t) > 0 \\ k_{p2}, & \text{otherwise.} \end{cases} \tag{4.6}$$

The function u_{Fps1} returns real values in the interval $[0, k_{p2}]$, where 0 corresponds to completely closed and where k_{p2} is the glycerol permeability coefficient in a completely open Fps1 channel.

The output of the HOG branch, which corresponds to the HOG pathway dependent glycerol production, is expressed as

$$u_{HOG}(t) = \begin{cases} k_{HOG} \cdot e, & e(t) > 0 \\ 0, & \text{otherwise,} \end{cases} \tag{4.7}$$

where k_{HOG} is the gain of this branch.

The time delay accounting for transcription and translation in the HOG pathway is approximated by

$$\frac{d\tilde{u}_{HOG}}{dt} = \frac{1}{T_d}(u_{HOG}(t) - \tilde{u}_{HOG}(t)),$$

with $\tilde{u}_{HOG}(t)$ being the time delayed variable and T_d being the amount of time delay considered. As reported in [8], very simple proportional controllers have been used in order to reduce the complexity of the model, even though it is known that, for example, MAPK signalling pathways often exhibit a switch–like behaviour, Huang and Ferrell [13]. In the last section of this chapter we compare the dynamics of this model with those obtained by using a HOG controller implementing ultrasensitivity, Montefusco et al. [25] (Table 4.1). AQ1

4.3.1.3 The Glycerol Module

The exchange of internal and external glycerol, u_{Diff} over the Fps1 channel is modelled by using Fick's first law of diffusion as

$$u_{Diff}(t) = u_{Fps1}(t)\left(\frac{Gly(t)}{V(t) - V_b} - \frac{Gly_e(t)}{V_e}\right),$$

with V_e being the extra-cellular volume and Gly_e being the glycerol concentration in the extra-cellular compartment. Intra-cellular glycerol Gly production is expressed, combining the output of the two controllers described above, as

$$\frac{dGly}{dt} = \tilde{u}_{HOG}(t) - u_{Diff}(t)$$

Table 4.1 Model parameters: all volumes are scaled such that the initial volume of the cell is 1

Parameters		Bounds
k_{p1}	Water perm. coeff.	$[0.0052,\ 160]$ Osm^{-1}
k_{p2}	Fps1 control const.	$[0,\ \infty]$
T_d	Time delay	[5, 30] min
k_{HOG}	HOG control const.	$[0,\ \infty]$ Osm^{-1}
$Gly(0)$	Initial Gly	$[1.1\quad 5] \times 10^{-4}$
$P_i(0)$	Initial P_i	[0.6 0.7] Osm
$P_e(0)$	Initial P_e	[0.24 0.25] Osm
V_b	Non osmotic volume	[0.31 0.46]
$V^{P_t=0}$	V when $P_t = 0$	[0.5 0.99]
V_e	External volume	$[0.5\quad 5] \times 10^3$
Dependent parameters		Value
$V(0)$	Initial V - relative volume	1
$Gly_e(0)$	Initial Gly_e	$\frac{V_e Gly(0)}{(V(0)-V_b)}$
$P_t(0)$	Initial P_t	$P_i(0) - P_e(0)$
s	No. of osmolytes other than Gly	$P_i(0)(V(0) - V_b)$ -$Gly(0)$

Both Gly and Gly_e represent number of molecules (mol scaled by $V(0)$)

and extra-cellular glycerol, depending only on the diffusion over the Fps1 channel, is described by

$$\frac{dGly_e}{dt} = u_{Diff}(t).$$

4.3.2 Parameter Estimation and Results

The model contains 14 parameters, 4 of which are dependent, as given in Table 4.5. In [8], the other parameters are estimated by simulating the model and minimising the error defined as the sum of the squares of the difference between simulated, $X(t)$, and experimental time series data, $\hat{X}(t_i)$, for intra–cellular and total glycerol. The error for one time series is calculated as

$$\text{error} = \sum_i (X(t_i) - \hat{X}(t_i))^2. \tag{4.8}$$

The best parameters found are given in Table 4.2. To find a possible global minimum point of the error function, the authors in [8] evaluated several randomly chosen starting points in the feasible region of the parameter space. The research was continued for the sets of parameter with sufficient low error by using the function *fmincon* from the MATLAB Optimization Toolbox, MATLAB [22]. Figures 4.3 and 4.4 show the simulated data using the simple model devised in [8] and the parameter set given

Table 4.2 Optimized parameters by using the relation (4.8): the values of P_e and k_{p1} were fixed while the remaining 8 parameters were estimated from time series data

Parameters		Value
k_{p1}	Water perm. coeff.	1 Osm^{-1}
k_{p2}	Fps1 control const.	0.316
T_d	Time delay	8.61 min
k_{HOG}	HOG control const.	0.416 Osm^{-1}
$Gly(0)$	Initial Gly	2×10^{-4}
$P_i(0)$	Initial P_i	0.636 Osm
$P_e(0)$	Initial P_e	0.240 Osm
V_b	Non osmotic volume	0.368
$V^{P_t=0}$	V when $P_t = 0$	0.99
V_e	External volume	4.79×10^3

Gly represents number of molecules (mol scaled by $V(0)$)

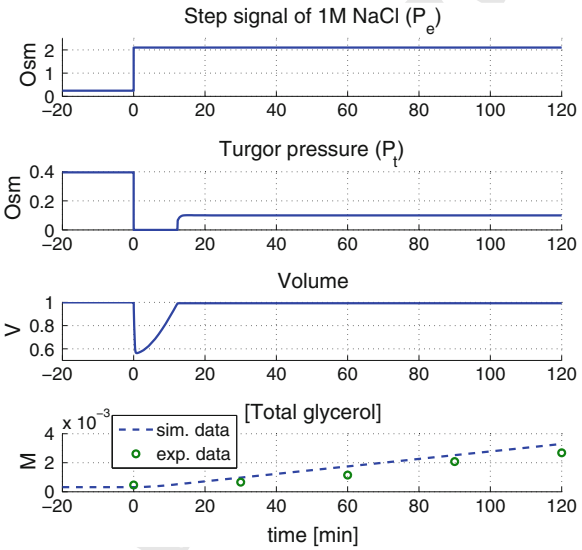

Fig. 4.3 Simulation of a step signal of $1M$ NaCl at $t = 0$. *Upper plot* external osmotic signal. *Second plot* the turgor pressure. *Third plot* the volume response. *Lower plot* the total glycerol concentration for the simulated (sim.) and experimental (exp.) data taken from [8]

in Table 4.2 and a comparison with the time-series experimental data. Figure 4.3 shows the simulation of the model by applying an osmotic stress of $1M$ NaCl at time $t = 0$, corresponding to an increase in the extra–cellular osmotic pressure by 1.86 Osm, while Fig. 4.4 shows the response to a double stress of $0.5M$ NaCl at $t = 0$ and $t = 30$. The simulated data show how the turgor pressure and volume drop immediately upon the osmotic stress. While the volume returns to approximately the same value as before the stress, the turgor pressure, the controlled variable, doesn't reach its previous value. The main reason for incomplete recovery is that the model para-

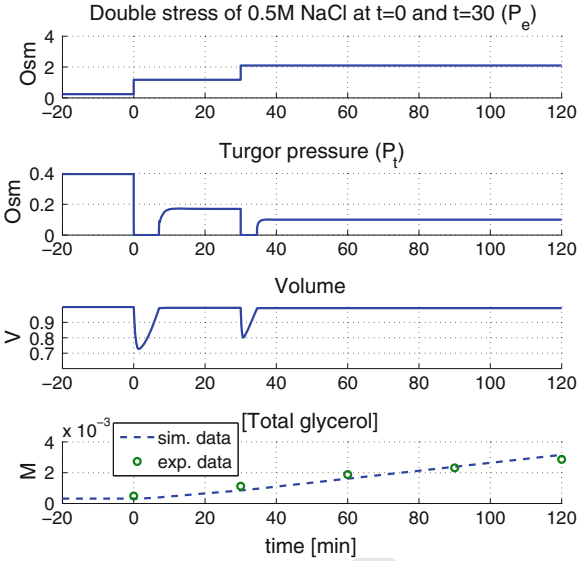

Fig. 4.4 Simulation of a double stress of $0.5M$ NaCl at $t = 0$ and $t = 30$. *Upper plot* external osmotic signal. *Second plot* the turgor pressure. *Third plot* the volume response. *Lower plot* the total glycerol concentration for the simulated (sim.) and experimental (exp.) data taken from [8]

meters are estimated by using the measured glycerol data, which are not sufficient for complete recovery of both volume and turgor pressure. The reason why volume and not turgor pressure is recovered is due to the high value of the estimated $V^{P_t=0}$, indicating a low elasticity of the cell wall. Therefore, turgor pressure is not recovered until the volume is almost completely recovered. For a lower value of $V^{P_t=0}$, the turgor pressure would be recovered faster and the volume slower. Figure 4.4 shows that the model can reproduce the regulatory behaviour of the system to a series of osmotic shocks. Moreover, it is able to predict the behaviour of modified strains. For example, Fig. 4.5 shows the simulation to an osmotic shock in a modified strain with constitutively open Fps1 (i.e. only one control mechanism via the HOG pathway). This test was experimentally demonstrated in [15]. To simulate this experiment we set $u_{Fps1} = k_{p2}$ (see Eq. (4.6)) and adjust the value of $Glyc(0)$ to obtain a realistic initial value of total glycerol. Figure 4.5 shows that the model correctly predicts the levels of total glycerol. Note, in particular, an over-production of the glycerol as experimentally measured (double production compared to wild type experiment) and a prolonged activation time of the HOG pathway (see Fig. 4d in [15]), that can not be explicitly observed using this model, since Hog1 is not a variable of the model, but implicitly deduced from the delay of volume recovery.

This model can therefore give us significant insight into the functioning of the system, and the results indicate that even such a simple model can predict the behaviour of different strains and the response to different input functions. It is also easier to understand and analyse than the detailed model developed in [15] (compare Fig. 4.1

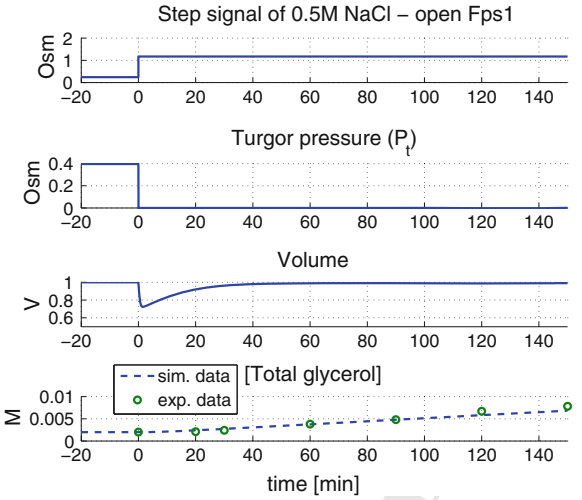

Fig. 4.5 Simulation of one osmotic stress of $0.5M$ NaCl at $t = 0$ in modified system (open Fps1). *Upper plot* external osmotic signal. *Second plot* the turgor pressure. *Third plot* the volume response. *Lower plot* the total glycerol concentration for the simulated (sim.) and experimental (exp.) data taken from [8]

with Fig. 4.2). However, detailed models are often important to completely understand a particular phenomena. For instance, in [15] the authors extracted novel information on the features of the system: the switch-like behaviour of the phosphorelay module consisting of three protein (Sln1, Ypd1 and Ssk1) that become more pronounced for higher number of components (see Fig. 2a in [15], where a comparison of the steady-state characteristics is performed for phosphorelay systems consisting of one, two and three proteins); and the main role of the phosphatases, that is to constantly counteract HOG pathway activation to set thresholds and reduce noise instead of providing a direct downregulation of the pathway.

4.4 Systems-Engineering Approaches

In this section we introduce some methods based on systems-engineering tools to better understand the dynamics of the osmo–adaptation response. In this area, important contributions have been produced by the group of van Oudenaarden. In a first work (see [24]), the authors analysed the dynamics of the system in the frequency domain, a feasible approach which allows the derivation of a concise model of the basic mechanisms of the osmoregulation, that emerge from an intricate network of interactions acting at very different time–scales, e.g. ligand binding or unbinding, phosphorylation, diffusion between compartments and transcription of genes. In [26], the authors later found that Hog1–dependent glycerol accumulation is crucial for the perfect adaptation of yeast to simple step increases of osmotic change,

suggesting that Hog1 may implement integral–feedback via an as yet–unknown role for protein-protein interactions that increase the internal osmolyte concentration.

4.4.1 A LTI System Identification

In this section we apply frequency domain analysis to derive a concise model of the HOG MAPK cascade in the budding yeast *S. cerevisiae*. Our treatment is mainly based on the results presented in [24]. After a hyper osmotic shock, membrane proteins trigger a signal transduction cascade that culminates in the activation of the MAPK Hog1. This activated protein, which is primarily cytoplasmic before the shock, is then imported into the nucleus, where it activates several transcription responses to osmotic stress. When the osmotic balance is restored, Hog1 is deactivated through dephosphorylation, thus allowing its export back in the cytoplasm. In order to identify the model, the input and the output of the system to be predicted have to be defined: in this case the input is the extra–cellular osmolyte concentration and the output is the concentration of active Hog1 protein. In [24] the input is manipulated by varying the salt concentration of the medium surrounding the cells, whereas the output is measured by estimating the localisation of Hog1 in the nucleus, $R(t)$, through fluorescence image analysis: the cellular localisation of Hog1-YFP, a yellow fluorescent protein fused to Hog1, and Nrd1-RFP, a red fluorescent protein fused to a strictly nuclear protein, are simultaneously monitored and $R(t)$ is measured as the nuclear to total Hog1 ratio in the cell ($R(t) = (< YFP >_{nucleus} / < YFP >_{cell})_{population}$, averaged over the 50–300 cells observed in the microscope's field of view).

The experiments are performed by applying pulse wave signals to the cells with different values of the period T_0, ranging from 2 to 128 min and they show that the steady-state response is approximately sinusoidal, with period T_0 (see Fig. 4.6). Using Fourier analysis, both the input and the output can be approximated as sine waves oscillating with a period $T_0 = 2\pi/\omega_0$. In particular, the experimental input, using a first harmonic approximation (see [5] pp. 26–30), can be written as

$$u(t) \approx 0.2\left(\frac{1}{2} + \frac{2}{\pi}\sin(\omega_0 t)\right) \tag{4.9}$$

and the steady-state response $R_\infty(t)$ as

$$R_\infty(t) = R_0 + A(\omega_0)\sin(\omega_0 t + \phi(\omega_0)), \tag{4.10}$$

where R_0 is the offset term and A and ϕ are two parameters that characterise the oscillations. A and ϕ are represented through the absolute value and phase of the complex number $\tilde{R}(\omega_0)$, respectively. This complex number is calculated from the Fourier coefficient of the experimental data, $R_\infty(t)$, taken for stimuli with period T_0 using the following relation:

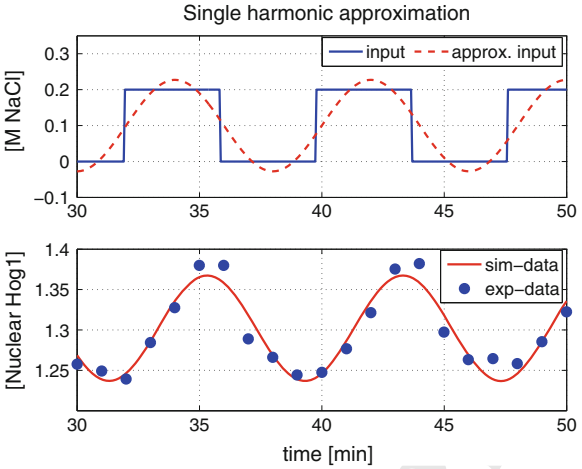

Fig. 4.6 *Upper plot* Pulse signal of 0.2 M NaCl with $T_0 = 8$ min and its approximation using the first harmonic. *Lower plot* the function $R_\infty(t)$ (sim.) defined by (4.11) and fitted to the experimental (exp.) measurements of nuclear Hog1 enrichment taken from [24]

$$\tilde{R}(\omega_0) = 2 \int_{nT_0}^{(n+m)T_0} \frac{\exp^{-i\omega_0 t} R_\infty(t)}{mT_0} dt, \tag{4.11}$$

The amplitude of the signal, defined as $A(\omega_0) = |\tilde{R}(\omega_0)|$, represents half the distance from the peak to the trough of the output sine wave. The phase parameter, $\phi(\omega_0)$, can be written implicitly as $\frac{\tilde{R}(\omega_0)}{|(\tilde{R}(\omega_0)|} \exp^{i(\phi(\omega_0)-\pi/2)}$. The parameter n is chosen so that the system is allowed to approach steady state before computing $\tilde{R}(\omega_0)$. The parameter m, which represents the number of periods over which the Fourier transform is computed, is set to be at least two for periods less than 64 min. For periods greater than or equal to 64 min, it is found that the first period is a good representation of the steady state oscillations and thus $\tilde{R}(\omega_0)$ is computed over this period alone. However, the values $A(\omega_0)$ and $\phi(\omega_0)$ can be computed for different values of ω_0 by fitting the parameters of the Eq. (4.11) to the experimental time response as shown in the lower plot of Fig. 4.6 for $\omega_0 = 2\pi/8$ rad/min. The resulting frequency response is shown on the Bode plots in Fig. 4.7.

A predictive model can be identified from the available experimental data by using linear systems theory: a linear input–output relationship in Fourier space is defined by

$$\tilde{Y}(\omega) = A_0 \frac{\prod_{i=1}^{n}(z_n + i\omega)}{\prod_{i=1}^{n}(p_n + i\omega)} \tilde{U}(\omega), \tag{4.12}$$

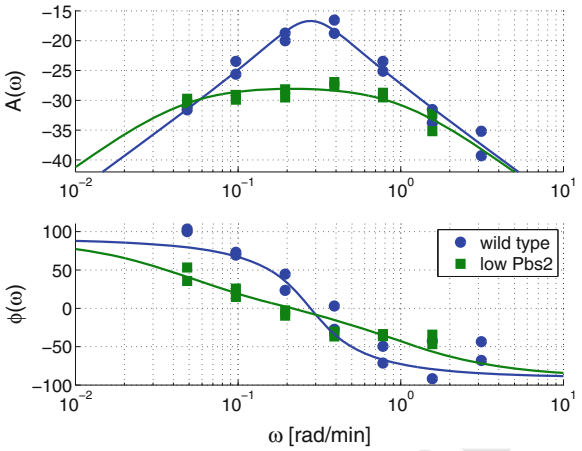

Fig. 4.7 The experimental data of the Fourier amplitude $A(\omega)$ and phase $\phi(\omega)$ (two measurements at each frequency), for wild type (*circles*) and underexpressed Pbs2 mutant (*squares*) strains, with the fitting models (*solid lines*). Experimental data taken from [24]

Table 4.3 Best-fitting parameters for the Eq. (4.13)

	p_1 [min^{-1}]	p_2 [min^{-1}]	A_0 [min^{-1}]
Wild type	$-0.1434 + 0.239i$	$-0.1434 - 0.239i$	0.3292
Low Psb2	-0.0466	-0.9755	0.3169

where $\tilde{Y}(\omega)$ and $\tilde{U}(\omega)$ are the output and input Fourier spectra, respectively, z_n are the n roots of the numerator of Eq. (4.12), also called *zeros*, and p_n are the n roots of the denominator, also called *poles*. The simplest such model from this class, that describes the experimental points in Fig. 4.7, exhibits a zero at the origin ($z_1 = 0$) and a pair of poles p_1 and p_2 yielding

$$(p_1 + i\omega)(p_2 + i\omega)\tilde{Y}(\omega) = (i\omega)A_0\tilde{U}(\omega)\,. \tag{4.13}$$

The best-fit parameters for the wild type and for the mutant (Pbs2 underexpression) strains are shown in Table 4.3. Applying the inverse Fourier transform (note a multiplication by $i\omega$ in Fourier domain corresponds to the derivative operator in time domain) the following relationship in the time–domain is given:

$$\ddot{y}(t) + (p_1 + p_2)\dot{y}(t) + (p_1 p_2)y(t) = A_0\dot{u}(t)\,. \tag{4.14}$$

The identified second-order LTI models, defined by the Eq. (4.13), are used to predict the response of the two strains to a step input of 0.2 M NaCl. Figure 4.8 shows the predicted responses of the two models and a comparison with the experimental measurements: the responses of the linear systems are offset by a constant value (1.23 M NaCl), which is the experimentally measured basal activity level of Hog1. The two models show a good qualitative match to the different sets of data for the two

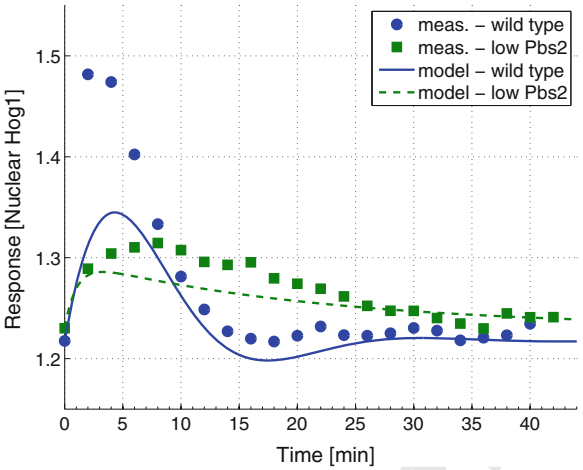

Fig. 4.8 Time domain response of the system to a step increase of 0.2 M NaCl: comparison of the responses predicted by the two linear models developed in the frequency domain vs the experimental measurements taken from [24]

yeast strains (the match is not perfect, since these are linear models of a process that will clearly also involve some nonlinear dynamics). Note that the wild type model exhibits a pair of complex conjugated poles and therefore the response is oscillatory, with a larger overshoot and a faster response than the low Pbs2 model, as expected from the experimental data. Indeed, the latter has two real poles, and thus exhibits a limited initial overshoot, a fast initial rise (due to the pole with small time constant) and a slow decay (caused by the large time constant associated with the other real pole). The identified LTI model can be written as a pair of differential equations, that is more readily interpreted in terms of biological process:

$$\begin{pmatrix} \dot{z}(t) \\ \dot{y}(t) \end{pmatrix} = \begin{pmatrix} a & b \\ c & d \end{pmatrix} \begin{pmatrix} z(t) \\ y(t) \end{pmatrix} + \begin{pmatrix} e \\ f \end{pmatrix} u(t) \tag{4.15}$$

with rate constants a, b, c, d, e and f. The variable $y(t)$ is assumed to represent the observable output of the system (the level of Hog1 activity), whereas the variable $z(t)$ represents the hidden state and $u(t)$ the osmotic stimulus. When these equations are simplified to remove the hidden variable $z(t)$, a single second order differential equation in $y(t)$ is obtained:

$$\ddot{y}(t) = (a+d)\dot{y}(t) + (bc - ad)y(t) + (ec - af)u(t) + f\dot{u}(t) \tag{4.16}$$

This equation is equivalent to the one in (4.14), if $f = A_0$, $ce = aA_0$ and $c \neq 0$. Substituting these relations in (4.15), we obtain the following system:

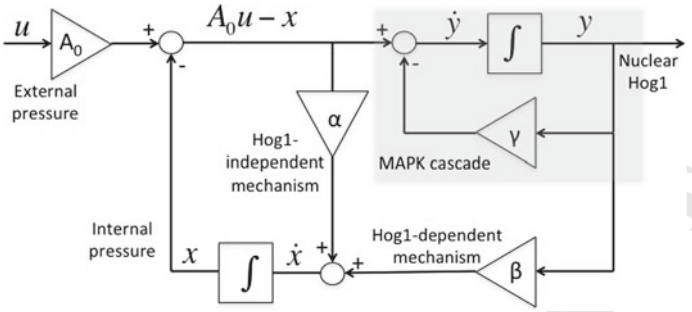

Fig. 4.9 Block diagram representation of the system (4.18): two negative feedback loops (Hog1-independent and Hog1-dependent mechanisms) act to reduce the difference between the stimulus, $A_0u(t)$, and the internal-state variable, $x(t)$, representing the internal pressure

$$\begin{pmatrix}\dot{z}(t)\\ \dot{y}(t)\end{pmatrix} = \begin{pmatrix}\frac{ce}{A_0} & b\\ c & d\end{pmatrix}\begin{pmatrix}z(t)\\ y(t)\end{pmatrix} + \begin{pmatrix}e\\ A_0\end{pmatrix}u(t) = \begin{pmatrix}\frac{e}{A_0} & b\\ 1 & d\end{pmatrix}\begin{pmatrix}A_0u(t)+cz(t)\\ y(t)\end{pmatrix}. \quad (4.17)$$

Defining $x(t) = -cz(t)$, $\alpha = -\frac{ec}{A_0}$, $\beta = -bc$ and $\gamma = -d$ the system (4.17) is written as

$$\begin{pmatrix}\dot{x}(t)\\ \dot{y}(t)\end{pmatrix} = \begin{pmatrix}\alpha & \beta\\ 1 & -\gamma\end{pmatrix}\begin{pmatrix}A_0u(t)-x(t)\\ y(t)\end{pmatrix} = \begin{pmatrix}\alpha(A_0u(t)-x(t))+\beta y\\ A_0u(t)-x(t)-\gamma y\end{pmatrix}. \quad (4.18)$$

Comparing this relation with the LTI model, we can equate coefficients to obtain the relations:

$$\alpha+\gamma = p_1+p_2, \qquad p_1 = \frac{1}{2}((\alpha+\gamma)+\sqrt{(\alpha-\gamma)^2-4\beta},$$

and

$$\alpha\gamma+\beta = p_1p_2, \qquad p_2 = \frac{1}{2}((\alpha+\gamma)-\sqrt{(\alpha-\gamma)^2-4\beta}.$$

The identified model, described by the relation (4.18), contains two negative feedback loops, which act to reduce the difference, $(A_0u(t)-x(t))$, between the stimulus, $A_0u(t)$, and the internal-state variable $x(t)$ (see Fig. 4.9). This enables us to assign a physical meaning also to the variable, $x(t)$: since the input is the external pressure, x represents the internal pressure. Moreover the model tells us that one feedback mechanism is mediated by the Hog1 MAPK pathway (βy changes x through the activity of the observable output y), whereas a second one is mediated by a pathway which is independent of Hog1. Since Hog1 is activated by Pbs2, we can derive useful insight by comparing the responses of the wild type strain with the mutant strain, in which Pbs2 is underexpressed (see Fig. 4.8). This comparison suggests that the feedback action provided by the Hog1 pathway is stronger,

producing a faster response. As discussed in Sect. 4.3, the hyperosmotic-shock response in yeast is regulated by two parallel mechanisms: 1) the Hog1-independent pathway activating the membrane protein Fps1 that quickly (<2 min) responds by decreasing the glycerol-export rate (see [19, 36]); 2) the Hog1-dependent pathway increasing the expression of Gpd1 and Gpd2 which accelerate the production of the glycerol over a longer time scale (>30min—see [2]). Although the topology of the model identified corresponds closely to that of the known biological system (see Fig. 4.9) the dynamic differences suggest that the MAPK Hog1 plays a role not only in the transcriptional regulation of glycerol producing proteins, but also in the control of the rapid accumulation of glycerol, consistent with previous studies (see [19, 36, 37]): from Fig. 4.8 the peak times of the responses of both wild type and mutant strains are less than 10 min and in both cases the response is much faster than the characteristic dynamics of gene expression. From this analysis the authors, in [24], have hypothesized that gene expression may be more important as a longer–time scale feedback in the hyperosmotic-shock response. To test this hypothesis, they stimulated cells with periodic pulses of NaCl (see Fig. S5 in [24]). The cells were shocked either in the absence or presence of cycloheximide, a small molecule that inhibits protein synthesis. They showed that cells respond very similarly to an initial pulse of osmolyte both in the absence or presence of cycloheximide. On the other hand, to adapt to subsequent pulses, cells need less time in the absence of cycloheximide and more in its presence. These results suggest that non transcriptional feedback mediates short–time scale osmolyte accumulation (see [8, 15, 28, 37]), whereas gene expression plays a role in osmolyte production only over longer time scales and for more intense shocks.

4.5 Perfect Adaptation in Yeast Osmoregulation

As shown in the last section the concise model developed by [24] is able to predict the Hog1 response by using only two differential equations. However, a detailed comparison of the LTI model's predictions with the experimental data sets shows that this model (only containing two negative feedback loops that control the rapid accumulation of glycerol) is too simple to fully reproduce the quantitative dynamics of the Hog1 nuclear enrichment when the cell are stimulated multiple times with periodic pulses of NaCl (see Figs. S8 and S9 in [40]). In particular, the experimental data sets and the model presented in [40] suggest that yeast can remember the first pulse of high osmolarity and needs less time to adapt to subsequent pulses of simulation. The LTI model developed by [24] fails to capture this dynamical property and, in [26], the same group proposed a revised concise LTI model by implementing an integral feedback mechanism which requires Hog1 kinase activity. They started with a minimalist model represented by the network diagram of Fig. 4.10, which aims to predicts the dynamics of the osmoregulation system with only a few key parameters, starting from input-output data, and, using biological measurements and engineering principles, to better understand the relation of its dynamics with the

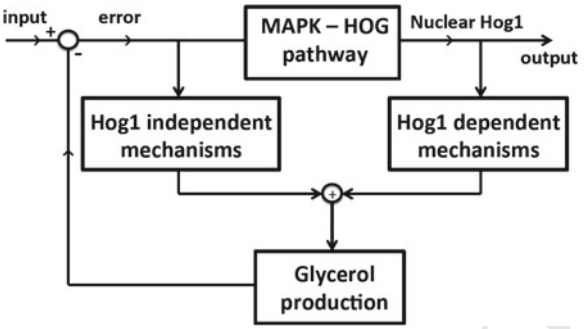

Fig. 4.10 Network diagram of the omsoregulation system presented in [26]

network topology. The authors represent in a subsystem all relevant reactions that determine the activation of the MAPK signalling pathway and the nuclear import of the activated protein Hog1 (MAPK signaling & nuclear import) and in another subsystem all the Hog1-dependent mechanisms that promote the glycerol production (Hog1-dependent mechanisms—such as the transcriptional activation of genes that encode enzymes involved in the glycerol production and potential protein-protein interaction initiated by Hog1 in the cytoplasm or nucleus that lead to glycerol accumulation). In contrast in the model of Fig. 4.2, developed by [8], the HOG pathway controller represents both the HOG signalling pathway, transcription/translation and the synthesis of enzymes involved in glycerol production.

4.5.1 Experimental Measurements for the Perfect Adaptation

In [26] the authors observed perfect adaptation of Hog1 nuclear enrichment in response to step increases of the extracellular osmolyte concentration (see Fig. 4.11 where step inputs of NaCl with different amplitude are applied and Fig. S3 in [26] where KCl and sorbitol are also used as osmolytes—in these and in the following figures of this section, Hog1 nuclear enrichment is defined as the relative change from the pre-shock level): this adaptation occurs with very low cell-to-cell variability and is robust to the signalling fidelity of the MAPK cascade. In particular, for different cells, the dynamics of Hog1 nuclear enrichment and cell volume are very similar in response to a step osmotic stress, with trends that closely follow the population average (see Fig. 2A, B in [26]). In fact, the cell-to-cell variability in unstressed cells is comparable to the one in osmo-stressed cells as shown in Fig. S2 in [26], further indicating that the intrinsic noise of signal propagation is low and suggesting that the experimental setup itself may be the predominant source of noise in the experimental data. Moreover, to demonstrate the robustness of this perfect adaptation, measurements of the Hog1 response have been performed in cells with compromised MAPK signalling, by controlling the expression of PBS2, which encodes the kinase of Hog1

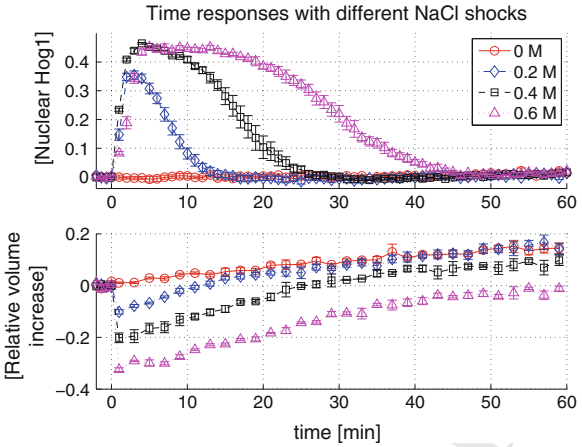

Fig. 4.11 Time measurements of Hog1 nuclear enrichment and volume to hyperosmotic shocks with indicated concentrations of salt. Data taken from [26]

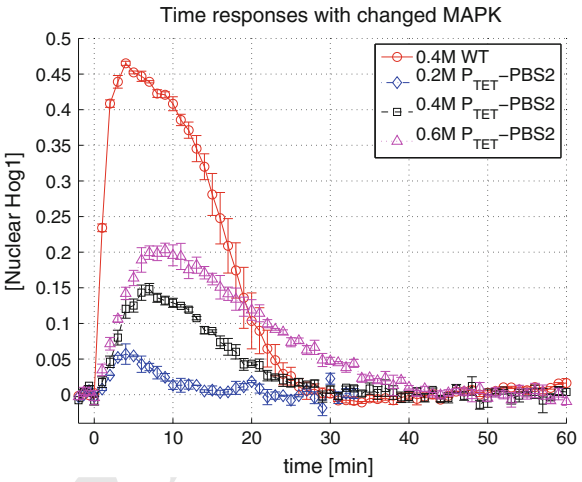

Fig. 4.12 Time measurements of Hog1 nuclear enrichment after changing the signaling fidelity of the MAPK cascade by controlling the expression of PBS2. Data taken from [26]

(see Fig. 4.12). Also in this case Hog1 nuclear enrichment still perfectly adapts and therefore we can say that the perfect adaptation is a robust property of the system and not a consequence of *ad hoc* parameter tuning. From these results, together with extensive theoretical analysis of adaptive systems in engineering, Muzzey et al hypothesised that this system implements integral feedback control in order to achieve robust perfect adaptation that does not require a precise tuning of system parameters such as protein levels or rate constant (see [14, 34, 39]).

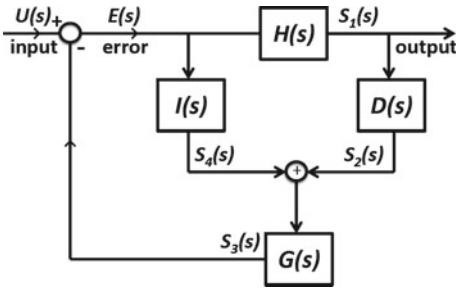

Fig. 4.13 Block diagram of the omsoregulation system presented in [26]. H represents all relevant reactions that link an osmotic disturbance at the membrane with Hog1 nuclear enrichment. D and I represent the Hog1-dependent and independent mechanisms for the glycerol accumulation, respectively. G represents the metabolic reactions involved in the glycerol synthesis

4.5.2 The Integral Feedback

The osmoregulation system is described by using the network diagram of Fig. 4.10, where the error indicates the deviation from the initial turgor pressure before applying the hyperosmotic stress. Figure 4.13 shows the corresponding block diagram of the osmosensing network of 4 subsystems denoted with G, D, H and I. H takes into account reactions that determine the activation of the MAPK signalling pathway and the nuclear import of the activated protein Hog1. D and I represent the Hog1-dependent and independent mechanisms that contribute to glycerol accumulation, respectively. Finally, G represents the metabolic reactions involved in the glycerol synthesis and any other reactions that promote glycerol accumulation. Approximating the network as being LTI, each subsystem can be described by a Laplace transform, or transfer function. In general a Laplace transform $F(s)$ of a function $f(t)$ is given by

$$F(s) = \int_0^\infty f(t) \exp^{-st} dt, \tag{4.19}$$

where s is a complex variable. The transfer function $S(s)$ of a LTI system is defined as $S(s) = Y(s)/U(s)$, where $U(s)$ and $Y(s)$ are the Laplace transform of the system input, $u(t)$, and output $y(t)$, respectively (see [5] pp. 30–33). The Laplace transform has the useful property that many relationships and operations in the time domain that require calculus can instead be performed using linear algebra in the s-domain (the differential equations in the time domain can be transformed into algebraic equations in the s-domain using the Laplace transform—these are then much easier to solve). By applying the final-value theorem (see [32] p. 43), the steady-state input and output are related via $y_{ss} = S(0)u_{ss}$, so perfect adaptation of the system output ($y_{ss} = 0$)

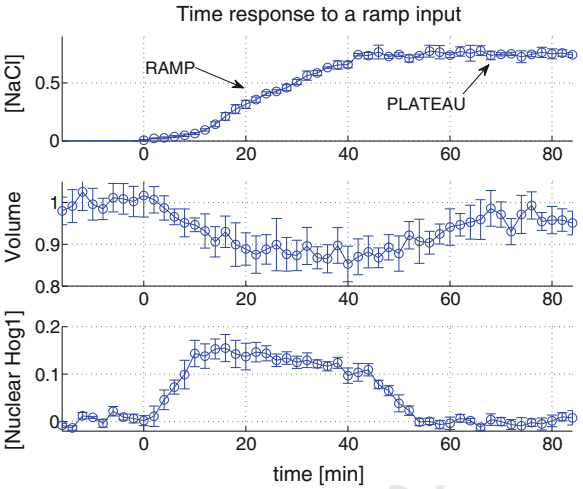

Fig. 4.14 Measurements of Hog1 nuclear enrichment and volume in an experiment where the salt concentration ramps upward over time, reaching a plateau after nearly 45 min. Experimental data taken from [26]

for an LTI system is equivalent to $S(0) = 0$, since the input is constant and nonzero. The input-error transfer function of the osmosensing system of Fig. 4.13 is given by

$$S_{ue}(s) = \frac{E(s)}{U(s)} = \frac{1}{1 + G(s)(D(s)H(s) + I(s))}, \tag{4.20}$$

where $G(s)$, $D(s)$, $H(s)$ and $I(s)$ are the transfer functions of the four subsystems in the network (see [5] pp. 42–46). We need that $S_{ue}(0) = 0$ to achieve perfect adaptation of the error to a step input. Therefore at least one of the four subsystems implements an integrator (its transfer function is given by $1/s$—see [5] p. 31—thereby allowing S_{ue} to be zero at $s = 0$). In general, a system contains at least one feedback loop with at least $n + 1$ integrators connected in series in order to achieve perfect adaptation to an input corresponding to the n-th integral of a step function, where n is a positive integer. Perfect adaptation to a step input, where $n = 0$, requires at least one integrator, perfect adaptation to a ramp input, where $n = 1$ since the ramp is the integral of a step, requires at least two integrators in series, and so on. In [26] the authors showed that neither cell volume nor Hog1 perfectly adapt in response to a ramp input, confirming that there is exactly one integrator in the osmosensing network (see Fig. 4.14). Therefore, the perfect adaptation of the error to a step input requires that only one of the four subsystems contains one integrator. Similarly, the input-output transfer function is given by

$$S_{us_1}(s) = \frac{S_1(s)}{U(s)} = \frac{H(s)}{1 + G(s)(D(s)H(s) + I(s))}. \tag{4.21}$$

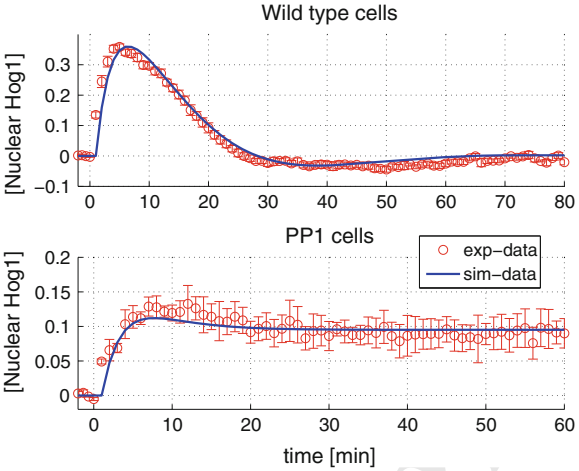

Fig. 4.15 Time domain response of the system (4.26) to a step increase of 0.4 M NaCl: comparison of the responses (sim.) predicted by the two models (wild type and PP1) vs the experimental (exp.) measurements taken from Fig. 5A in [26]

If $H(s)$ were the only subsystem performing integration, then Hog1 would not perfectly adapt ($S_{us_1}(0) \neq 0$). Therefore one or more of the other subsystems must contain an integrator to achieve perfect adaptation of Hog1, but the system only contains one integrator. In [26] it is shown that the cells lose perfect adaptation with PP1, a treatment to completely eliminate the Hog1 kinase activity, as the steady-state Hog1 accumulation ($s1_{ss}$ in Fig. 4.13) does not go back to the pre-stimulus level. Since the presence of PP1 disconnects the D subsystem from Hog1, the input-output transfer function of the system is modified as

$$S_{us_1}(s) = \frac{H(s)}{1 + G(s)I(s)}\,. \tag{4.22}$$

In this case Hog1 does not perfectly adapt, then the product $G(s)I(s)$ does not go to infinity at $s = 0$ ($S_{us_1}(0) \neq 0$), which implies that either the G and I subsystems both lack integrators, or one subsystem has an integrator but the other perfectly cancels the integrator (it is a differentiator with a transfer function equal to s—see [5] p. 31). If I contained the integrator, then the turgor pressure would perfectly adapt in the presence of PP1, and Hog1 likely would as well, but both properties are not observed in the data. If G were to act as an integrator, then cell volume and turgor pressure would continue to perfectly adapt for a nonzero input to the G subsystem. But, in the presence of PP1, the only input to subsystem G is the output from subsystem I, as subsystem D is disconnected. Thus, no volume recovery observed in PP1-treated cells would only occur if the output of subsystem I prematurely goes to zero (i.e. if it were a differentiator). As explained in [26], this observation would require that all Hog1-independent mechanisms completely desensitize within approximately 20 min (i.e. the time needed for Hog1 nuclear enrichment to reach steady state in PP1 cells—

see the lower plot of Fig. 4.15) despite persistence in their stimulus (i.e. the acute loss of turgor pressure). On the basis of this argument, it is extremely improbable that subsystem G acts an integrator. Therefore, the combination of all findings points to D as the subsystem with the only integrator in the feedback loop. Moreover, in PP1 cells, levels of total glycerol and extracellular glycerol are measured over time in the presence and absence of osmotic shock (see [26]): in the absence of salt shock, glycerol synthesis is increased as well as glycerol leakage; in the presence of osmotic shock, glycerol leakage is rapidly and transiently diminished, as in wild type cells, whereas the absence of Hog1 kinase activity prevents an increase in glycerol synthesis, unlike in wild type cells. These data suggest that Hog1 kinase activity plays a critical role in rapidly regulating glycerol synthesis but not its leakage as in [38].

Note from Fig. 4.12 (see also Fig. 3D in [26]) that the time-integral of the Hog1 scales linearly with the shock strength. If the system were composed only of reactions modelled with linear dynamics, then the result that D subsystem is an integrator would be trivial. However, this result is valid also when the other subsystems are nonlinear stable systems without integrators (see Fig. 4.12 where the fact that the peak Hog1 amplitude saturates as a function of salt is an evidence of nonlinear dynamics in the H subsystem). If it is assumed that the error perfectly adapts and the the steady-state output of the I subsystem is zero when its steady-state input is zero, then 1) the net change induced by the system in the steady-state input of the G subsystem simply equals the time-integral of Hog1, 2) the net change in the output of G must equal the net change in the system input in order for the error to go to zero. If the G subsystem were perfectly linear, then its output would be directly proportional to its input at steady state and so the time-integral of Hog1 would be directly proportional to the magnitude of the osmostress (despite potential nonlinearities in the H and I subsystems). This relationship is almost exactly what Fig. 3D in [26] shows, except that the line relating the integral of Hog1 nuclear enrichment to the magnitude of the osmostresses does not cross the origin. This difference may be due to nonlinearities in the input-output steady-state function of subsystem G that become evident for osmostresses of small magnitude (<0.2 M NaCl).

Finally, in order to validate these results, a LTI system can be used to implement the concise model represented by the block diagram of Fig. 4.13. The subsystems of the osmosensing network can be represented as follows: H and G as first-order systems where the corresponding transfer functions $H(s) = \frac{k_h}{s+\gamma_h}$, with gain k_h and time constant γ_h^{-1}, and $G(s) = \frac{1}{s+\gamma_g}$ with time constant γ_g^{-1}, I as a scalar α_i (i.e. $I(s) = \alpha_i$) and D as an integrator with gain α_d (i.e. $D(s) = \frac{\alpha_d}{s}$). Therefore the Laplace transform of the output, $S_1(s)$, of the H subsystem is defined as:

$$S_1(s) = \frac{k_h}{s+\gamma_h} E(s) = \frac{k_h}{s+\gamma_h}(U(s) - S_3(s)), \tag{4.23}$$

where the Laplace function error $E(s) = U(s) - S_3(s)$, with $U(s)$ and $S_3(s)$ the Laplace functions of the input $u(t)$ of the system and the output $s_3(t)$ of subsystem

Table 4.4 Best-fitting parameters for the system (4.26)

	k_h [min^{-1}]	γ_h [min^{-1}]	γ_g [min^{-1}]	α_d [min^{-1}]	α_i [min^{-1}]
Wild type	0.496	0.369	0.119	0.0106	0.0806
PP1	0.147	0.369	0.119	0	0.0806

G, respectively. We can obtain the rate equation for the output s_1 (corresponding to measured Hog1 nuclear enrichment) in the time domain applying the inverse Laplace transform of the following relation, by rewriting the Eq. (4.23):

$$s S_1(s) = -\gamma_h S_1(s) - k_h S_3(s) + k_h U(s)\,. \tag{4.24}$$

By applying the property that the derivative operator with respect to time correspond to a multiplication by s in the s-domain (see [5] p. 31), the inverse Laplace transform of (4.24) follows as:

$$\dot{s_1}(t) = -\gamma_h s_1(t) - k_h s_3(t) + k_h u(t) \tag{4.25}$$

In the same way, we can obtain the rate equations for the outputs s_2 and s_3 of the corresponding subsystems D and G. Then the following system of differential equations is obtained:

$$\begin{pmatrix} \dot{s_1}(t) \\ \dot{s_2}(t) \\ \dot{s_3}(t) \end{pmatrix} = \begin{pmatrix} -\gamma_h & 0 & -k_h \\ \alpha_d & 0 & 0 \\ 0 & 1 & -(\alpha_i + \gamma_g) \end{pmatrix} \begin{pmatrix} s_1(t) \\ s_2(t) \\ s_3(t) \end{pmatrix} + \begin{pmatrix} k_h \\ 0 \\ \alpha_i \end{pmatrix} u(t)\,. \tag{4.26}$$

Figure 4.15 shows the response of two strains (wild type and PP1 cells) to a step input of 0.4 M NaCl. Table 4.4 reports the best set of parameters that fit the experimental data. For the PP1 experiment we set $\alpha_d = 0$ to break the connection between Hog1 and the D subsystem. The simulations show how the devised model is able to capture the dynamics of the system and produces an excellent match to the experimental data.

4.6 The Role of Ultrasensitivity

As shown above, systems and control theory provides a highly useful approach to abstract complex biological systems that seem to operate with similar goals as engineered control systems, and the osmoregulation system in yeast is a prime example of this. The models here presented, by combing proportional and integral feedback controllers capture the key dynamics of a homeostatic system like osmoregulation in yeast, but they do not shed light on how the evolution of such a biological control system can proceed to result in integral feedback control. In the following we explore the possible role of ultrasensitivity in osmoregulation. Indeed, it has been well-

documented that the upstream signalling pathways involved in this system implement high levels of ultrasensitivity, however, the role of such high gain in producing the observed perfect adaptation is not clear. Therefore, we extend the proportional controller model presented in [8] for this system with the implementation of ultrasenstivity, Montefusco [25].

4.6.1 Ultrasensitive Model and Parameters

The mathematical model used for our analysis is the same as that presented in Sect. 4.3, apart from allowing the Hog controller to be non-linear (see Fig. 4.2). Indeed, in this case, the output of the HOG branch, which corresponds to the HOG pathway dependent glycerol production, is expressed as

$$u_{HOG}(t) = \begin{cases} k_{HOG} \cdot f(e), & e(t) > 0 \\ 0, & \text{otherwise}, \end{cases} \tag{4.27}$$

where the control function is given by

$$f(e) = \frac{e(t)^n}{\beta e(t)^n + K^n}, \tag{4.28}$$

with $\beta = 1$ and K and n being the nonlinear Hill function variables. We have thus modifed the control law for the HOG pathway, compared to the model in [8], to allow for a non-linear controller response. This is inspired by the fact that MAPK systems, of which the HOG pathway is an example, often show Hill type responses, Huang and Ferrell [13]. The performance of the nonlinear controller is contrasted with the proportional controller given in [8], where $\beta = 0$ and $K = n = 1$. Our model contains 16 parameters as reported in Table 4.5. However, four of these are dependent parameters which do not need to be constrained. The other parameters are estimated by simulating the model with different osmotic shocks and minimising the error, defined by Eq. (4.5), and time adaptation corresponding to the time required by the cell to approximately return to its volume before the stress (see the definition in the next subection). For the optimization, we use a hybrid Genetic Algorithm (GA) (see [18]), that combines the most well-known type of evolutionary algorithm with local gradient-based algorithms (see [7, 10]). We use the function *ga* from the MATLAB Global Optimization Toolbox, MATLAB [23], and *fmincon* from the MATLAB Optimization Toolbox, MATLAB [22], as the local algorithm. By the optimisation procedure some parameters do not significantly change their values, therefore, they are fixed equal to the values estimated in [8], except for $V^{P_t=0}$, which is set to 0.8, the value of the volume at zero P_t according to a recent study presented in [31]. AQ2

The cost function used for the parameter estimation is given by

Table 4.5 Model parameters: all volumes are scaled such that the initial volume of the cell is 1

Parameters		Bounds
k_{p1}	Water perm. coeff.	[0.0052 160] Osm^{-1}
k_{p2}	Fps1 control const.	[0 10]
T_d	Time delay	[5 30] min
k_{HOG}	HOG control const.	[0 2] Osm^{-1}
K	Hill const.	[0 0.01 2]
n	Hill exponent	[0 4]
Fixed parameters		Value
$Gly(0)$	Initial Gly	2×10^{-4}
$P_i(0)$	Initial P_i	0.636 Osm
$P_e(0)$	Initial P_e	0.24 Osm
V_b	Non osmotic volume	0.368
$V^{P_t=0}$	V when $P_t = 0$	0.8
V_e	External volume	4.79×10^3
Dependent parameters		Value
$V(0)$	Initial V - relative volume	1
$Gly_e(0)$	Initial Gly_e	$\frac{V_e Gly(0)}{(V(0)-V_b)}$
$P_t(0)$	Initial P_t	$P_i(0) - P_e(0)$
s	No. of osmolytes other than Gly	$P_i(0)(V(0) - V_b)$ -$Gly(0)$

Both Gly and Gly_e represent number of molecules (mol scaled by $V(0)$)

$$\min_x J, \tag{4.29}$$

where

$$J = J_p + J_v + J_t \tag{4.30}$$

is a sum of three scalar functions: J_p is the turgor pressure error, J_v is the difference between the desired and the effective volume and J_t is the response time of the system after the perturbation.

4.6.2 Results: Ultrasensitive Versus Proportional Controller

In our adaptation of the model developed by [8], we particularly consider the observed ultrasensitivity in the HOG branch of the system. This branch was originally modeled as a proportional control in [8], which we have replaced here by a Hill-type function to model ultrasensitivity (see Eqs. (4.27) and (4.28)). We then compare the performance of this new model against the original model. In particular, we evaluate the two different controllers—proportional (Pr) and ultrasensitive (Us)—by simulating their dynamics with different stress inputs (see Fig. 4.16) and optimizing their

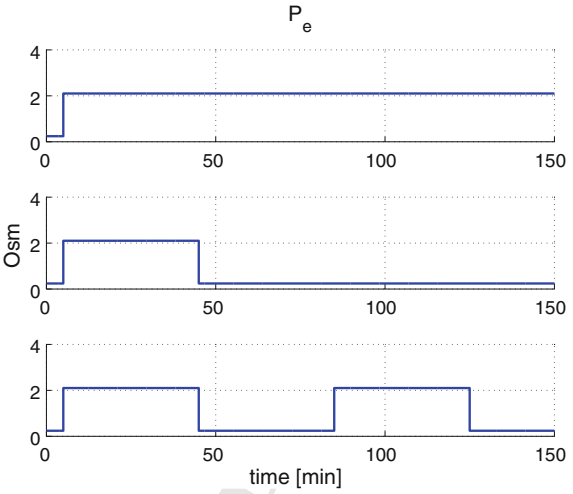

Fig. 4.16 Different osmotic stresses. *Upper plot* a constant step of 1M NaCl at $t = 5$ min corresponding to an increase of P_e equal to 1.96 Osm. *Middle plot* single pulse signal at t =5 min with duration of 40 min of 1M NaCl. *Lower plot* double pulse signal at $t_1 = 5$ and $t_2 = 85$ min, both with duration of 40 min and amplitude of 1M NaCl

parameters for optimum response (i.e. minimal deviation of cell volume and turgor pressure in presence of an osmo-schock, see Sect. 4.6.1 for details). We repeat this procedure for different levels of overall sensitivity (i.e. gain) of the HOG branch and different types of osmo-shock sequences and evaluate the tests by using two different performance indices: adaptation precision and adaptation time. The adaptation precision is defined as

$$X_a = \prod_i X_{s,i}, \tag{4.31}$$

where $X_{s,i}$ is the steady state value of the variable X (volume V or turgor pressure P_t) after the i-th perturbation. Since the initial volume is set to unity, this measure gives 1 for perfect adaptation. Deviations from 1 indicate inability of the system to perfectly adapt volume to pre-perturbation levels. The time adaptation, T_a, defined as

$$T_a = \sum_i t_{a,i}, \tag{4.32}$$

where $t_{a,i}$ is the time required by the system to reach 85 % of the volume V after the i-th osmotic stress. Figure 4.17 shows the results of the two controllers by applying three different osmotic stresses: constant step, single pulse and double pulse. For all different inputs the ultrasensitive controller achieves better and faster adaptation irrespective of the level of overall gain. The better performance is particularly significant when overall gain is limited to lower values, where the ultrasensitive controller achieves almost 2-fold faster responses. Indeed, using a a Hill function within the HOG branch allows us to effectively achieve a steeper response from this branch compared to a linear function for any given error (see Eqs. (4.27) and (4.28)). Thus, the controller acts faster and more strongly, allowing quicker and fuller recovery of

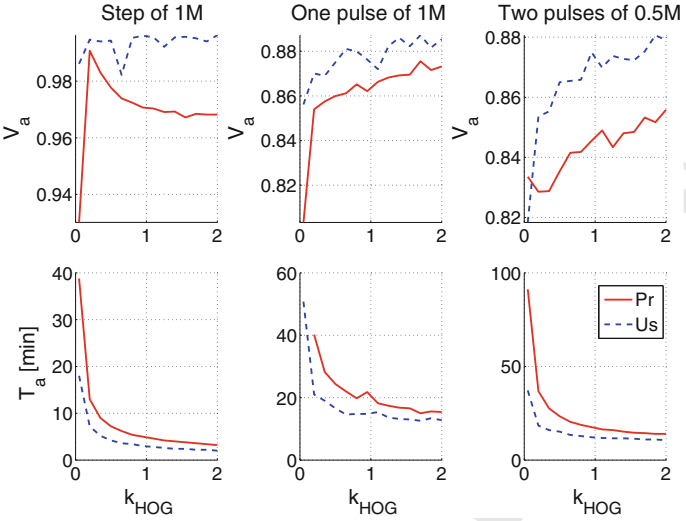

Fig. 4.17 Performance comparison between the proportional (Pr) and ultrasensitive (Us) controllers by applying different shocks: first column, a step of 1M of NaCl; second column, 1 pulse of 1M; third column, 2 pulses of 0.5M. V_a close to 1 indicates the capability of the system to adapt. T_a indicates the time adaptation

Table 4.6 Optimized parameters for a given k_{HOG} with a double pulse signal of 1M of NaCl

k_{HOG}	Optimized parameters—Pr/Us						Us	
	k_{p1}		T_d		k_{p2}		K	n
	Pr	Us	Pr	Us	Pr	Us		
0.65	93	155	5	5	0.43	0.96	0.17	3.53
1.1	159	124	5	5	0.69	1.17	0.23	3.78
1.55	0.36	134	5	5	0.9	1.61	0.23	3.8
2	155	159	5	5	1	1.54	0.25	3

the system. This insight is in line with the optimized parameters for both controllers as reported in Table 4.6: in most cases, the optimal parameters for the ultrasensitive controller result in a very steep Hill function that produces maximal outputs for even small error values. Of the other free parameters of the model, we note that certain parameters are optimized differently for the two controllers. For example, the permeability coefficient k_{p1}, which controls water flow in the model (see Eq. (4.2)) is usually optimized to higher values in the ultrasensitive controller compared to the proportional controller. This parameter affects the sensitivity of the system, as faster water movement can allow both a high volume reduction for a given osmo-shock and also fast recovery. Given its fast dynamics, the ultrasensitive controller can "afford" this parameter to become higher compared to the proportional controller.

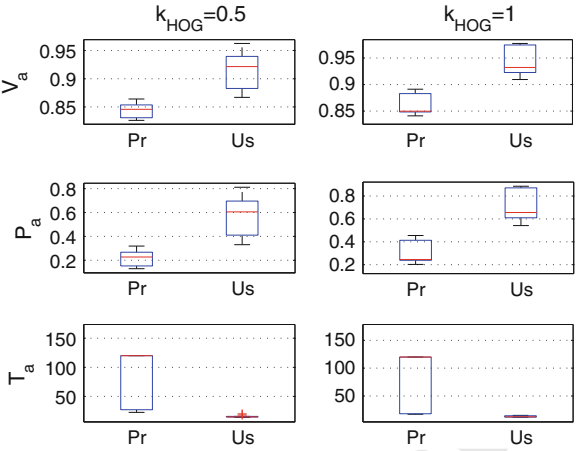

Fig. 4.18 Sensitivity analysis using the box-and-whisker representation (*median–middle line*, the 25th and 75th percentile—*lower* and *upper lines* of the box, and the outliers (crosses)) by fixing k_{HOG} and Hill function parameters ($K = 0.05$, $n = 3.5$) and applying one pulse signal of 1M of NaCl. The first column of each boxplot reports the results for the proportional (Pr) controller, the second column the results for the ultrasensitive (Us) controller. The system robustly adapts if V_a and P_a are close to 1. T_a indicates the time adaptation. Similar results are obtained with different Hill function parameters ($K = 0.2$, $n = 2$)—see Fig. 7 in [25]

Such differences between the optimal model parameters for the two controllers suggest that implementation of ultrasensitivity might allow more freedom in the other parameters of the model or allow them to be in a more favorable regime. To test the former possibility, we perform a simple sensitivity analysis for the two controllers. Given a certain gain, and Hill function parameters, we evaluate the adaptation precision and time of the two controllers for a set of 100 randomly generated parameters. Figure 4.18 shows that the ultrasensitive controller achieves much more robust adaptation performance than the proportional controller according to these two criteria.

As discussed above, the performance increase of the ultrasensitive controller over the proportional one stems from its high sensitivity to the error due to the Hill function. The incorporation of the Hill function, however, can also allow development of thresholds in the system. In particular, the ultrasensitive controller can be tuned as a filter allowing responses only to signals of certain magnitude or duration. To test this hypothesis, we devise an alternative cost function for the optimization procedure and optimize the system towards functioning as a filter. The new cost function is given by $J_n = J - J_{glyc}$, where J is defined by the Eq. (4.30) and J_{glyc} represents the glycerol production upon the signal of limited duration. Figure 4.19 shows the performance for a signal with a first short and then long duration pulse. The ultrasensitive controller ignores the first pulse and responds to the second by tuning the Hill parameters, whereas the proportional controller model is not able to response to the second signal (the permeability coefficient k_{p1}, that affects the sensitivity of the system, is equal to the lower bound).

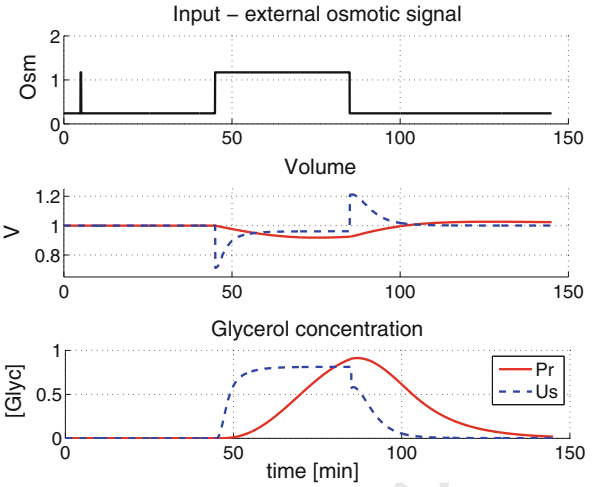

Fig. 4.19 Response to a signal with a short and long pulse duration, assuming $k_{HOG} = 0.25$. *Upper plot* external osmotic signal. *Second plot* the volume response for the proportional (Pr) controller and the ultrasensitive (Us) controller model. *Lower plot* the glycerol concentration for both the models

In conclusion, we show, using a previously developed proportional control model of the osmoergulation incorporating two main and distinct branches (HOG and channel branches), that ultrasensitivity in the HOG branch allows better overall performance. We find that the primary effect of ultrasensitivity in the HOG branch is an increase in the response speed of the system and consequently in its adaptation precision. In addition to this, however, we find that ultrasensitivity provides also a non-trivial flexibility to the system parameters. By increasing the speed of overall system responses, ultrasensitivity in the HOG branch allows sensitivity to be increased in the other branch of the system. In the absence of ultrasensitivity, fast (i.e. highly sensitive) regulation of the glycerol exchange branch limits the cell's adaptability through the HOG branch (i.e. glycerol production). With ultrasensitivity in glycerol production, the other system parameters can be increased or varied more freely, without compromising performance. Moreover, by increasing the gain of the HOG branch, the system with a proportional HOG controller is able to improve the performance in terms of adaptation, but there is a presence of overshoot in the system response, whereas ultrasensitivity in the HOG branch allows to avoid this phenomena (we do not consider the overshoot to compute the performance). Note that for large values of the error ($e > 1$), a proportional branch may have a higher gain than an ultrasensitive one and, if $K > 1$, the gain of the proportional controller will always be higher, but this is not the case here because the error never goes above 1, given the system parameters (the absolute maximum value of the error is $P_t(0)$). The ultrasensitive response in the HOG branch also allows tuning of the overall system response towards certain signal regimes. In other words, the control system can be tuned to filter out signals below a threshold and respond only when volume decreases cross

this threshold. Considering that glycerol production is potentially highly costly for the cell, this ability of the system could give an evolutionary advantage by allowing cells to ignore short lived or low doses of osmo-shock.

4.7 Conclusions

The results illustrated in this chapter demonstrate the power of applying engineering principles to the analysis of the osmoregulation system in yeast. Gennemark et al. [8] proposed a simple model that describes the essential physics and biology of osmoregulation. This model has been abstracted from another more detailed model, developed by [15], by focusing on fewer components which allow the reproduction of the main dynamics of the system: the cell controls the biophysical system (in particular in terms of volume and turgor pressure) by using two proportional controllers, which act in parallel and regulate the glycerol production and the glycerol outflow (see Fig. 4.2). This simple model captures the main dynamical features of the osmoadaptive response by predicting the behaviour of different strains (wild type and modified) with different inputs and confirming the existence of two mechanisms of control (see Sect. 4.3). Note, however, that in general the volume adapts while the turgor pressure does not, because the model parameters are estimated using only glycerol concentration measurements which are not sufficient for complete recovery of both volume and turgor pressure. Therefore the model does not show robust adaptation, since the adaptation requires a careful tuning of the system parameters.

The group of van Oudenaarden, using frequency domain analysis, identified a minimal model represented by a LTI system with only two dynamics variables (see Sect. 4.4). Then, they estimated the biological quantities corresponding to the two relevant variables of the LTI model and, using these results, deduced the network diagram of Fig. 4.10. Using biological measurements and engineering principles, they showed that the robust perfect adaptation of Hog1 nuclear enrichment and cell volume (as turgor pressure) results from one integrating mechanism that requires Hog1 kinase activity and regulates the glycerol synthesis (see Sect. 4.5).

The models of Figs. 4.2 and 4.10 seem similar at a "formal" level but they are quite different from the system theoretical point of view. The model of the group of Van Oudenaarden is inferred by employing the Hog measurements (the output of the model) and contains one branch of control modelled with exactly one integrator. Instead, in Gennemark's model, the Hog protein cannot be observed (it is not a variable of the model and the Hog controller does not have a direct biological correspondence) and the two branches of control are modelled using simple proportional controllers. The model could be modified by adding measurable variables, for example Hog1, but this would obviously increase the complexity of the model.

Interesting additional results were recently presented in [20], where the authors investigated which network topologies in a generic signalling network are capable of robust adaptation. In particular, they used a network of three nodes as a minimal framework, where there is a first node that receives the input, a second that transmits

the output and a third that can play diverse regulatory roles. They found that all the networks containing one of the following two motifs achieve adaptation: negative feedback loop with a buffering node and incoherent feedforward loop with a "proportioner" node.

Despite the many striking insights that have been produced into the yeast osmoregulation system by the above analyses, it is still not clear how the evolution of biological control systems of this type can result in integral feedback, and in our recent work we investigated a heretofore largely unexplored alternative control system which also appears to be able to achieve perfect adaptation. In particular, we extended the proportional control model developed by [8] with the implementation of ultrasensitivity and found that a proportional controller implementing ultrasensitivity allows more precise and faster adaptation of cell volume following an osmo-shock. Further, the ultrasensitive controller can be tuned as a filter, where the proportional controller could not, and thereby allows responses to signals only above a certain threshold (see Sect. 4.6). These results provide new insights on the potential role of gain in biological systems and should be of interest to synthetic biologists attempting to design robust biomolecular control systems.

References

1. Alberts B, Bray D, Lewis J, Raff M, Roberts K, Watson JD (1994) Molecular biology of the cell. Garland Publishing, Inc., New York
2. Albertyn J, Hohmann S, Thevelein JM, Prior BA (1994) Gpd1, which encodes glycerol-3-phosphate dehydrogenase, is essential for growth under osmotic stress in saccharomyces cerevisiae, and its expression is regulated by the high-osmolarity glycerol response pathway. Mol Cell Biol 14(6):4135–4144
3. Blossey R, Bodart JF, Devys A, Goudon T, Lafitte P (2012) Signal propagation of the MAPK cascade in Xenopus oocytes: role of bistability and ultrasensitivity for a mixed problem. J Math Biol 64(1–2):1–39
4. Buchler NE, Cross FR (2009) Protein sequestration generates a flexible ultrasensitive response in a genetic network. Mol Syst Biol 5:272
5. Cosentino C, Bates DG (2011) Feedback control in systems biology. CRC Press (Taylor & Francis), Boca Raton
6. El-Samad H, Goff JP, Khammash M (2002) Calcium homeostasis and parturient hypocalcemia: an integral feedback perspective. J Theor Biol 214(1):17–29
7. Fleming PJ, Purshouse RC (2002) Evolutionary algorithms in control systems engineering: a survey. Control Eng Pract 10:1223–1241
8. Gennemark P, Nordlander B, Hohmann S, Wedelin D (2006) A simple mathematical model of adaptation to high osmolarity in yeast. Silico Biol 6(3):193–214
9. Gervais P, Beney L (2001) Osmotic mass transfer in the yeast saccharomyces cerevisiae. Cell Mol Biol (Noisy-le-grand) 47(5):831–839
10. Goldberg DE (1989) Genetic algorithms in search, optimization and machine learning. Addison-Wesley, Boston
11. Goldbeter A, Koshland DE (1981) An amplified sensitivity arising from covalent modification in biological systems. PNAS 78(11):6840–6844
12. Ho SN (2006) Intracellular water homeostasis and the mammalian cellular osmotic stress response. J Cell Physiol 206(1):9–15. doi:10.1002/jcp.20445, http://dx.doi.org/10.1002/jcp.20445

13. Huang CY, Ferrell JE (1996) Ultrasensitivity in the mitogen-activated protein kinase cascade. PNAS 93(19):10078–10083
14. Ingalls BP, Yi T, Iglesias P (2006) Using control theory to study biology. In: Knabe JF, Nehaniv CL, Schilstra MJ (eds) System modeling in cellular biology. MIT Press, Cambridge, pp 243–267
15. Klipp E, Nordlander B, Krger R, Gennemark P, Hohmann S (2005) Integrative model of the response of yeast to osmotic shock. Nat Biotechnol 23(8):975–982. doi:10.1038/nbt1114, http://dx.doi.org/10.1038/nbt1114
16. Kltz D, Burg M (1998) Evolution of osmotic stress signaling via map kinase cascades. J Exp Biol 201(Pt 22):3015–3021
17. Levin RL, Ushiyama M, Cravalho EG (1979) Water permeability of yeast cells at sub-zero temperatures. J Membr Biol 46(2):91–124
18. Lobo FG, Goldberg D (1996) Decision making in a hybrid genetic algorithm. IlliGAL Report No 96009
19. Luyten K, Albertyn J, Skibbe WF, Prior BA, Ramos J, Thevelein JM, Hohmann S (1995) Fps1, a yeast member of the mip family of channel proteins, is a facilitator for glycerol uptake and efflux and is inactive under osmotic stress. EMBO J 14(7):1360–1371
20. Ma W, Trusina A, El-Samad H, Lim WA, Tang C (2009) Defining network topologies that can achieve biochemical adaptation. Cell 138(4):760–773. doi:10.1016/j.cell.2009.06.013, http://dx.doi.org/10.1016/j.cell.2009.06.013
21. Markevich NI, Hoek JB, Kholodenko BN (2004) Signaling switches and bistability arising from multisite phosphorylation in protein kinase cascades. J Cell Biol 164(3):353–359
22. MATLAB (1990) Optimization Toolbox User's Guide. Natick, MA
23. MATLAB (2004) Global Optimization Toolbox User's Guide. Natick, MA
24. Mettetal JT, Muzzey D, Gómez-Uribe C, van Oudenaarden A (2008) The frequency dependence of osmo-adaptation in saccharomyces cerevisiae. Science 319(5862):482–484. doi:10.1126/science.1151582, http://dx.doi.org/10.1126/science.1151582
25. Montefusco F, Steinacher A, Akman OE, Bates DG, Soyer OS (2012) On the role of ultrasensitivity in biomolecular control systems. In: Proceedings of the 51st IEEE CDC conference, Maui, Hawaii.
26. Muzzey D, Gómez-Uribe CA, Mettetal JT, van Oudenaarden A (2009) A systems-level analysis of perfect adaptation in yeast osmoregulation. Cell 138(1):160–171
27. Ni XY, Drengstig T, Ruoff P (2009) The control of the controller: molecular mechanisms for robust perfect adaptation and temperature compensation. Biophys J 97(5):1244–1253
28. Proft M, Struhl K (2004) Map kinase-mediated stress relief that precedes and regulates the timing of transcriptional induction. Cell 118(3):351–361. doi:10.1016/j.cell.2004.07.016, http://dx.doi.org/10.1016/j.cell.2004.07.016
29. Reed RH, Chudek JA, Foster R, Gadd GM (1987) Osmotic significance of glycerol accumulation in exponentially growing yeasts. Appl Environ Microbiol 53(9):2119–2123
30. Rep M, Krantz M, Thevelein JM, Hohmann S (2000) The transcriptional response of saccharomyces cerevisiae to osmotic shock. hot1p and msn2p/msn4p are required for the induction of subsets of high osmolarity glycerol pathway-dependent genes. J Biol Chem 275(12):8290–8300
31. Schaber J, Adrover MA, Eriksson E, Pelet S, Petelenz-Kurdziel E, Klein D, Posas F, Goksör M, Peter M, Hohmann S, Klipp E (2010) Biophysical properties of Saccharomyces cerevisiae and their relationship with HOG pathway activation. Eur Biophys J 39(11):1547–1556
32. Skogestad S, Postlethwaite I (1996) Multivariable feedback control: analysis and design. Wiley, Chichester
33. Smith AE, Zhang Z, Thomas CR (2000) Wall materials properties of yeast cells: part 1. Cell measurements and compression experiments. Chem Eng Sci 55:2031–2041
34. Sontag E (2003) Adaptation and regulation with signal detection implies internal model. Syst Contr Lett 50:119–126
35. Sunder S, Singh AJ, Gill S, Singh B (1996) Regulation of intracellular level of na+, k+ and glycerol in saccharomyces cerevisiae under osmotic stress. Mol Cell Biochem 158(2):121–124

36. Tams MJ, Luyten K, Sutherland FC, Hernandez A, Albertyn J, Valadi H, Li H, Prior BA, Kilian SG, Ramos J, Gustafsson L, Thevelein JM, Hohmann S (1999) Fps1p controls the accumulation and release of the compatible solute glycerol in yeast osmoregulation. Mol Microbiol 31(4):1087–1104
37. Thorsen M, Di Y, Tngemo C, Morillas M, Ahmadpour D, Van der Does C, Wagner A, Johansson E, Boman J, Posas F, Wysocki R, Tams MJ (2006) The mapk hog1p modulates fps1p-dependent arsenite uptake and tolerance in yeast. Mol Biol Cell 17(10):4400–4410. doi:10.1091/mbc.E06-04-0315, http://dx.doi.org/10.1091/mbc.E06-04-0315
38. Westfall PJ, Patterson JC, Chen RE, Thorner J (2008) Stress resistance and signal fidelity independent of nuclear mapk function. Proc Natl Acad Sci U S A 105(34):12212–12217. doi:10.1073/pnas.0805797105, http://dx.doi.org/10.1073/pnas.0805797105
39. Yi TM, Huang Y, Simon MI, Doyle J (2000) Robust perfect adaptation in bacterial chemotaxis through integral feedback control. PNAS 97(9):4649–4653
40. Zi Z, Liebermeister W, Klipp E (2010) A quantitative study of the Hog1 MAPK response to fluctuating osmotic stress in Saccharomyces cerevisiae. PLoS One 5(3):e9522

Author Queries

Chapter 4

Query Refs.	Details Required	Author's response
AQ1	Please check and confirm the inserted citation of Table 4.1 is correct. If not suggest an alternate citation.	
AQ2	Please note that table captions were same for Tables 4.1 and 4.5. So check and provide.	

MARKED PROOF

Please correct and return this set

Please use the proof correction marks shown below for all alterations and corrections. If you wish to return your proof by fax you should ensure that all amendments are written clearly in dark ink and are made well within the page margins.

Instruction to printer	*Textual mark*	*Marginal mark*
Leave unchanged	··· under matter to remain	
Insert in text the matter indicated in the margin		New matter followed by or
Delete	through single character, rule or underline or through all characters to be deleted	or
Substitute character or substitute part of one or more word(s)	through letter or through characters	new character or new characters
Change to italics	under matter to be changed	
Change to capitals	under matter to be changed	
Change to small capitals	under matter to be changed	
Change to bold type	under matter to be changed	
Change to bold italic	under matter to be changed	
Change to lower case	Encircle matter to be changed	
Change italic to upright type	(As above)	
Change bold to non-bold type	(As above)	
Insert 'superior' character	through character or where required	or under character e.g. or
Insert 'inferior' character	(As above)	over character e.g.
Insert full stop	(As above)	
Insert comma	(As above)	
Insert single quotation marks	(As above)	or and/or or
Insert double quotation marks	(As above)	or and/or or
Insert hyphen	(As above)	
Start new paragraph		
No new paragraph		
Transpose		
Close up	linking characters	
Insert or substitute space between characters or words	through character or where required	
Reduce space between characters or words	between characters or words affected	